

Searching for minimum in dependence of squared speed-of-sound on collision energy

Fu-Hu Liu^{a,1}, Li-Na Gao^a, and Roy A. Lacey^{b,2}

^a*Institute of Theoretical Physics, Shanxi University, Taiyuan, Shanxi 030006, China*

^b*Departments of Chemistry & Physics, Stony Brook University, Stony Brook, NY 11794, USA*

Abstract: Experimental results of the rapidity distributions of negatively charged pions produced in proton-proton (p - p) and beryllium-beryllium (Be-Be) collisions at different beam momentums, measured by the NA61/SHINE Collaboration at the super proton synchrotron (SPS), are described by a revised (three-source) Landau hydrodynamic model. The squared speed-of-sound parameter c_s^2 is then extracted from the width of rapidity distribution. There is a local minimum (knee point) which indicates a softest point in the equation of state (EoS) appearing at about $40A$ GeV/ c (or 8.8 GeV) in c_s^2 excitation function [the dependence of c_s^2 on incident beam momentum (or center-of-mass energy)]. This knee point should be related to the searching for the onset of quark deconfinement and the critical point of quark-gluon plasma (QGP) phase transition.

Keywords: Rapidity distribution of negatively charged pions, speed of sound, revised (three-source) Landau hydrodynamic model, knee point

PACS: 13.85.-t, 13.85.Ni, 25.75.Dw, 24.10.Nz, 24.10.Pa

1 Introduction

Comparing with the relativistic heavy ion collider (RHIC) in USA [1–3] and the large hadron collider (LHC) in Switzerland [4, 5], the fixed target experiments performed at the super proton synchrotron (SPS) in Switzerland [6, 7] present relatively simple and clean collisions process. The multiplicity in collisions at the SPS is also low comparing with those at the RHIC and LHC. As one of the “first day” measurement quantities, the rapidity (pseudorapidity) distributions of charged particles are reported by experimental collaborations [1–7]. These distributions give us a chance to analyze longitudinal picture of particle productions. At the same time, based on the rapidity distributions, one can extract other information such as the penetrating (stopping) power of projectile (target) nucleus, energy and rapidity losses of projectile nucleus, energy and particle densities of interacting region, and so forth.

As a measurement of particle density and mean free path, the squared speed-of-sound parameter which characterizes partly the formation of matters in interacting region can be extracted from the width of Gaussian rapidity distribution described by the Landau

¹E-mail: fuhuliu@163.com; fuhuliu@sxu.edu.cn

²E-mail: Roy.Lacey@Stonybrook.edu

hydrodynamic model [8–18]. Generally, the rapidity spectra obtained in collisions at the SPS, RHIC, and LHC are not simply Gaussian distributions. Instead, two Gaussian distributions, one in the backward (target) region and the other in the forward (projectile) region, are needed to fit the experimental data [6, 19, 20]. However, the two-Gaussian distribution implies that there is no central source at midrapidity, which seems unbelievable. According to the three-source relativistic diffusion model [21–24], a central source arisen from interactions between low-momentum gluons in both target and projectile should be located at midrapidity, a target-like (projectile-like) source arisen from interactions between valence quarks in the target (projectile) and low-momentum gluons in the projectile (target) are expected to appear in the backward (forward) rapidity region.

To extract the squared speed-of-sound parameter so that the formation of matters can be characterized by an alternative method, we need the Landau hydrodynamic model [8–10] and its improved or simplified version [11–18] in the descriptions of rapidity distributions. In fact, the Landau hydrodynamic model is not good enough to fit the whole rapidity range. In our recent work [25, 26], we have revised the Landau hydrodynamic model [8–18] to a three-source situation. The rapidity distributions measured in experiments are then described by three Gaussian distributions. This picture is consistent with the three-source relativistic diffusion model [21–24].

In this paper, we use the revised (three-source) Landau hydrodynamic model [25, 26] to describe the rapidity distributions of negatively charged pions produced in proton-proton (p - p) and beryllium-beryllium (Be-Be, exactly ^7Be - ^9Be) collisions at different beam momentums measured by the NA61/SHINE Collaboration at the SPS. Combining with our previous works [25, 26], we observe the dependence of squared speed-of-sound on collision energy in a wide range.

The rest of this paper is structured as follows. The model is shortly described in section 2. Results and discussion are given in section 3. In section 4, we summarize our main observations and conclusions.

2 The model

The revised (three-source) Landau hydrodynamic model used in the present work can be found in our previous work [25, 26]. To give a short and clear description of the model, we introduce the main results of the model in the following.

The Landau hydrodynamic model [8–18] results approximately in a Gaussian rapidity distribution which does not exactly describe the experimental data [6, 19, 20]. We have revised the model to three sources: a central source which locates at midrapidity and covers the rapidity range as wide as possible, and a target (projectile) source which locates in the backward (forward) region and revises the rapidity distribution from the central source [25, 26]. The experimental rapidity distributions are then described by three Gaussian functions. And based on the three Gaussian functions, the experimental pseudorapidity distributions can be described by a method which makes a distinction between rapidity and pseudorapidity.

According to the Landau hydrodynamic model [8–18] and our revision [25, 26], the rapidity distribution, dN_{ch}/dy , of charged particles produced in a given source in high

energy collisions can be described by a Gaussian function

$$\frac{dN_{ch}}{dy} = \frac{N_0}{\sqrt{2\pi}\sigma_X} \exp \left[-\frac{(y - y_X)^2}{2\sigma_X^2} \right], \quad (1)$$

where σ_X , y_X , and N_0 denote the width, peak position, and normalization constant, respectively; $X = C$, T , and P are for the central, target, and projectile sources, respectively. The experimental result is in fact a sum weighted by the three Gaussian functions.

The relation between σ_X and the squared speed-of-sound $c_s^2(X)$ is

$$\sigma_X = \sqrt{\frac{8}{3} \frac{c_s^2(X)}{1 - c_s^4(X)}} L, \quad (2)$$

where $L = \ln(\sqrt{s_{NN}}/2m_p)$ is the logarithmic Lorentz contraction factor which is independent of X , $\sqrt{s_{NN}}$ denotes the center-of-mass energy per pair of nucleons in nucleus-nucleus collisions and is simplified to \sqrt{s} in p - p collisions, and m_p denotes the rest mass of a proton. From Eq. (2), $c_s^2(X)$ is expressed by using σ_X to be

$$c_s^2(X) = \frac{1}{3\sigma_X^2} \left(\sqrt{16L^2 + 9\sigma_X^4} - 4L \right). \quad (3)$$

In the above extractions of σ_X and $c_s^2(X)$ from the rapidity distribution, we distinguish accurately the rapidity and pseudorapidity distributions [25, 26]. In the case of representing the pseudorapidity distribution in experiment, we also extract σ_X and $c_s^2(X)$ from the hidden rapidity distribution. Our treatment ensures the method of extraction being concordant.

3 Results and discussion

Figure 1 presents the rapidity distributions, dn/dy , of negatively charged pions produced in p - p and ${}^7\text{Be}$ - ${}^9\text{Be}$ collisions at the SPS. For p - p collisions, the incident momenta for Figures 1(a)–1(e) are 20, 31, 40, 80, and 158 GeV/ c , respectively, which correspond to $\sqrt{s} = 6.3, 7.7, 8.8, 12.3$, and 17.3 GeV, respectively. For ${}^7\text{Be}$ - ${}^9\text{Be}$ collisions, the incident momenta for Figures 1(a)–1(e) are 20A, 31A, 40A, 75A, and 150A GeV/ c , respectively, which correspond to $\sqrt{s_{NN}} = 6.3, 7.7, 8.8, 11.9$, and 16.8 GeV, respectively. The symbols represent the experimental data of the NA61/SHINE Collaboration [6, 7] and the curves are our results fitted by the revised (three-source) Landau hydrodynamic model. Different centrality classes (0–5%, 5–10%, 10–15%, and 15–20%) for ${}^7\text{Be}$ - ${}^9\text{Be}$ collisions are presented by different symbols marked in the panels. The values of fit parameters, σ_C , σ_T ($= \sigma_P$), y_C , rapidity shift Δy ($= y_C - y_T = y_P - y_C$), relative contribution k_T of the target source ($= k_P$, the relative contribution of the projectile source), and normalization constant N_0 , are listed in Table 1 with the values of χ^2 per degree of freedom (dof). The last two columns in Table 1 present the values of $c_s^2(C)$ and $c_s^2(T)$ [$= c_s^2(P)$], which are calculated from Eq.(3) due to σ_X . Both $c_s^2(C)$ and $c_s^2(T)$ [$= c_s^2(P)$] are in the units of c^2 , where c is the speed of light in vacuum. One can see that the model describes approximately the experimental data in most cases.

To see clearly the relation between parameter and energy, Figures 2(a) and 2(b) give the dependences of main free parameter σ_X and extracted parameter $c_s^2(X)$ on $\sqrt{s_{NN}}$, re-

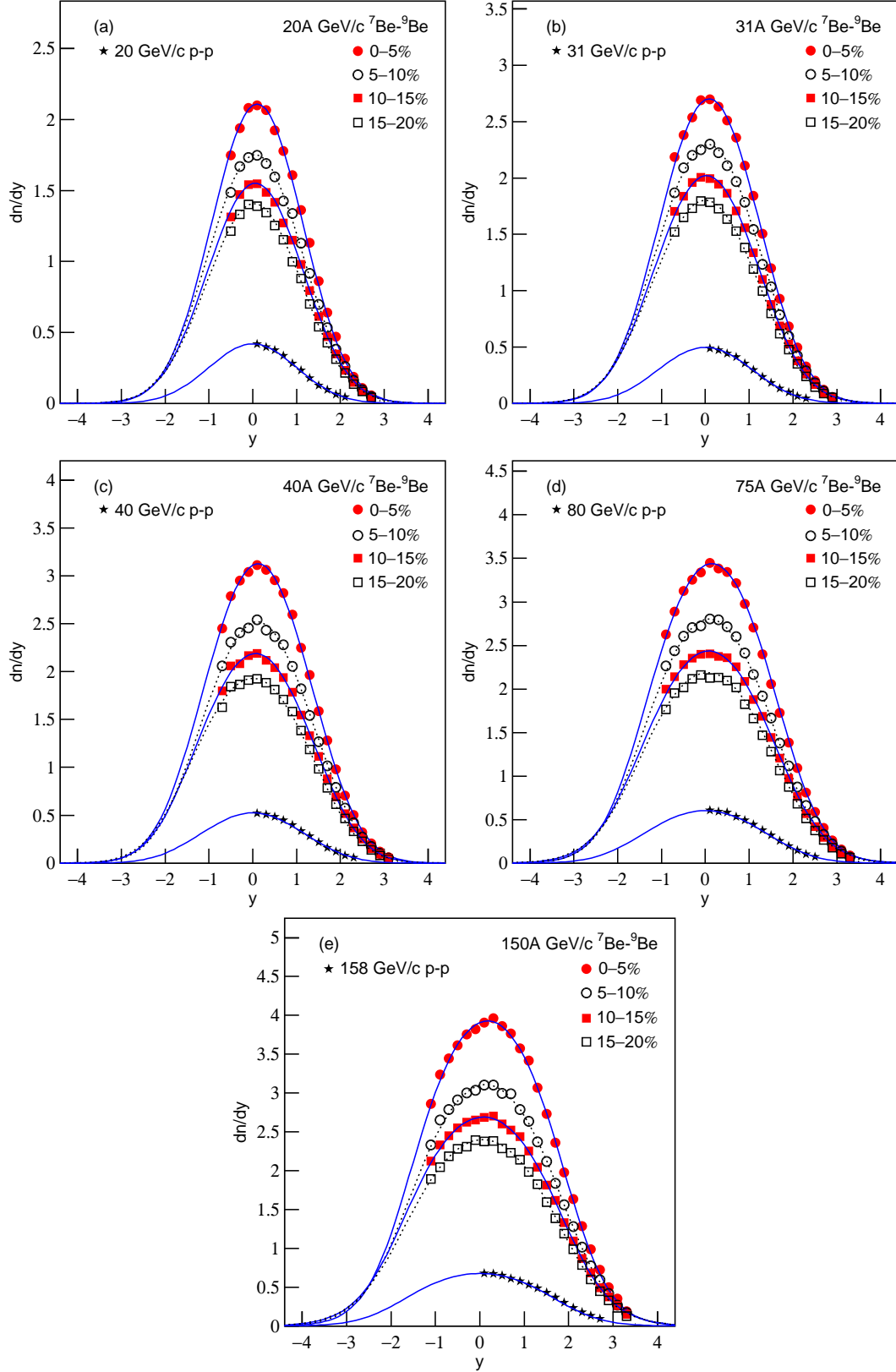


Figure 1. Rapidity distributions of negatively charged pions produced in p - p and ${}^7\text{Be}$ - ${}^9\text{Be}$ collisions at the SPS. Figures 1(a)–1(e) correspond to different beam momenta marked in the panels. The symbols represent the experimental data of the NA61/SHINE Collaboration [6, 7] and the curves are our results fitted by the revised (three-source) Landau hydrodynamic model.

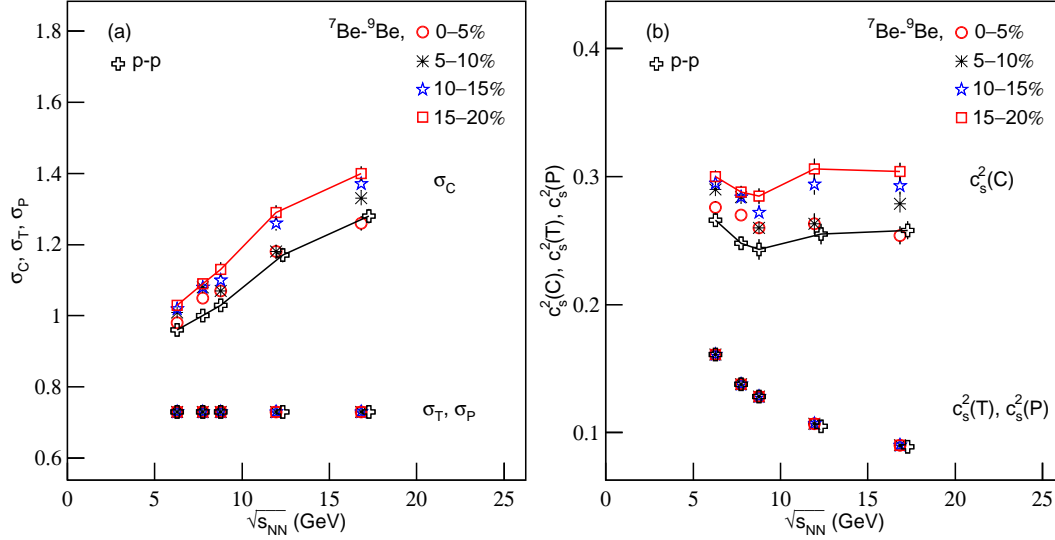


Figure 2. Dependences of (a) σ_X and (b) $c_s^2(X)$ on $\sqrt{s_{NN}}$. The symbols represent the values listed in Table 1 and the line segments for two cases are given for guiding the eyes. Different symbols correspond to different types (centralities) of collisions.

spectively. The results corresponding to p - p collisions and ${}^7\text{Be}$ - ${}^9\text{Be}$ collisions with different centrality classes are displayed by different symbols, which reflect a part of parameter values listed in Table 1. The line segments for p - p collisions and for ${}^7\text{Be}$ - ${}^9\text{Be}$ collisions with centrality class 15–20% are given for guiding the eyes. One can see that σ_C increases with increase of $\sqrt{s_{NN}}$, σ_T (σ_P) does not show a change with $\sqrt{s_{NN}}$, $c_s^2(C)$ shows itself a local minimum (knee point) which indicates a softest point in the equation of state (EoS) at $\sqrt{s_{NN}} = 8.8$ GeV, and $c_s^2(T)$ [$c_s^2(P)$] decreases with $\sqrt{s_{NN}}$. The dependences of other parameters (y_C , Δy , k_T , and N_0) on energy are not analyzed due to trivialness.

To study the knee point in detail, Figures 3(a) and 3(b) show σ_C and $c_s^2(C)$ excitation functions [the dependences of σ_C and $c_s^2(C)$ on $\sqrt{s_{NN}}$] respectively, where the results for p - p and Be-Be collisions at lower energies (≤ 17.3 GeV) are taken from Figure 2 (Table 1) and the results for p - p , proton-antiproton (p - \bar{p}), copper-copper (Cu-Cu), gold-gold (Au-Au), and lead-lead (Pb-Pb) collisions at higher energies (≥ 19.6 GeV) are taken from our previous works [25, 26]. Different symbols represent different collisions, which are marked in the panels. The symbols with large size denote central collisions, and the symbols with small size denote non-central collisions. The centrality classes for Cu-Cu collisions are from 0–3% to 50–55% [27]; for Au-Au collisions are from 0–3% to 45–50% (maximum 40–45% at 19.6 GeV) [27]; and for Pb-Pb collisions are from 0–5% to 20–30% [28]. The line segments for p - p collisions at SPS and higher energies are given for guiding the eyes, and the two dotted lines in Figure 3(b) show $c_s^2(C) = 1/3$ and $1/2$ respectively. One can see that at higher energies σ_C increases with increase of $\sqrt{s_{NN}}$ and most $c_s^2(C)$ are between $1/3$ and $1/2$ [a few $c_s^2(C)$ are beyond $1/2$ due to statistical fluctuations].

In particular, one can see some detailed laws in $c_s^2(C)$ excitation function [the dependence of $c_s^2(C)$ on $\sqrt{s_{NN}}$]: i) In the lower energy range, $c_s^2(C)$ decreases with increase of $\sqrt{s_{NN}}$, then the first knee point appears at $\sqrt{s_{NN}} = 8.8$ GeV, afterwards $c_s^2(C)$ increases

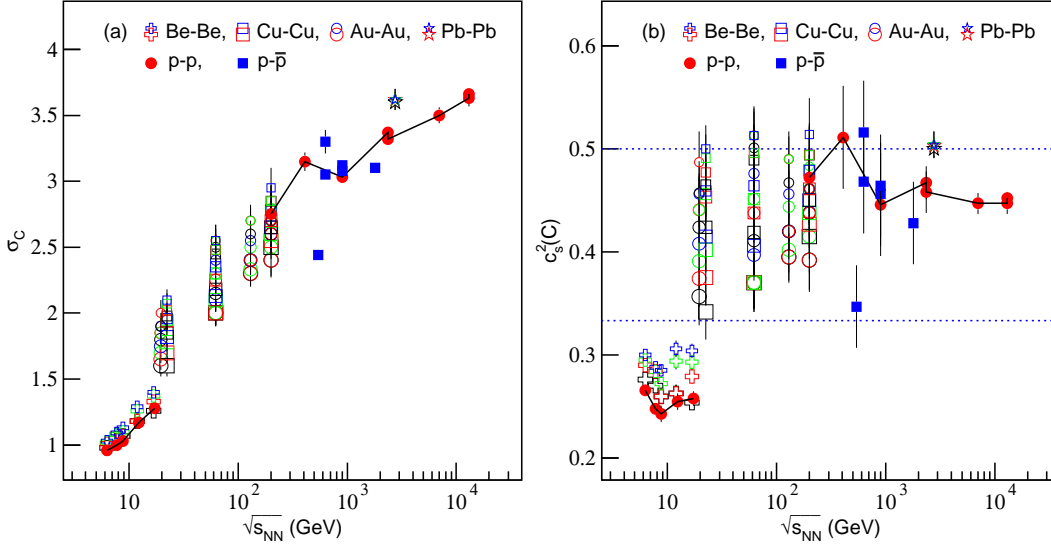


Figure 3. Dependences of (a) σ_C and (b) $c_s^2(C)$ on $\sqrt{s_{NN}}$. The symbols represent the values listed in Table 1 (for the energy range ≤ 17.3 GeV), and taken from our previous work [25, 26] (for the energy range ≥ 19.6 GeV). The line segments for p - p collisions at SPS and higher energies are given for guiding the eyes, and the two dotted lines in Figure 3(b) show $c_s^2(C) = 1/3$ and $1/2$ respectively.

with increase of $\sqrt{s_{NN}}$. ii) From 17.3 to 19.6 GeV, $c_s^2(C)$ has a jump from ≤ 0.3 to $1/3$ – $1/2$. iii) In the higher energy range, $c_s^2(C)$ seems not related to $\sqrt{s_{NN}}$, a saturation appears. The first knee point is a local minimum which indicates a softest point in the EoS. As the predecessor of $c_s^2(C)$, σ_C increases always with increase of $\sqrt{s_{NN}}$. We do not observe a softest point in the EoS in σ_C excitation function. These abundant phenomenons should be related to the searching for the onset of deconfinement of the quarks and gluons in proton-proton collisions, and the critical point of phase transition from hadronic matter to quark-gluon plasma (QGP) in nucleus-nucleus collisions.

The softest point (8.8 GeV) obtained in the present work is compatible with the previous works [29, 30] which used the Landau hydrodynamic model and the ultra-relativistic quantum molecular dynamics hybrid approach and indicated the softest point locating in the energy range from 4 to 9 GeV. Other works which study dependences of ratio of numbers of positive kaons and pions (K^+/π^+) [20, 31, 32], chemical freeze-out temperature (T_{ch}) [31, 32], mean transverse mass minus rest mass ($\langle m_T \rangle - m_0$) [31], and ratio of widths of experimental negative pion rapidity distribution and Landau hydrodynamic model prediction [$\sigma_y(\pi^-)/\sigma_y(\text{hydro})$] [32] on $\sqrt{s_{NN}}$ show knee point around 7–8 GeV. A wiggle in the excitation function of a specific reduced curvature of the net-proton rapidity distribution at midrapidity is expected in the energy range from 4 to 8 GeV [33, 34]. However, the searching for the onset of quark deconfinement and the critical point of QGP phase transition is a complex process [35]. The relation between the softest point and onset of deconfinement is still an open question. Analyses of more other experimental data are needed so that they can be confirmed each other.

As for the jump of $c_s^2(C)$ from ≤ 0.3 to $1/3$ – $1/2$ when $\sqrt{s_{NN}}$ increases from 17.3 to

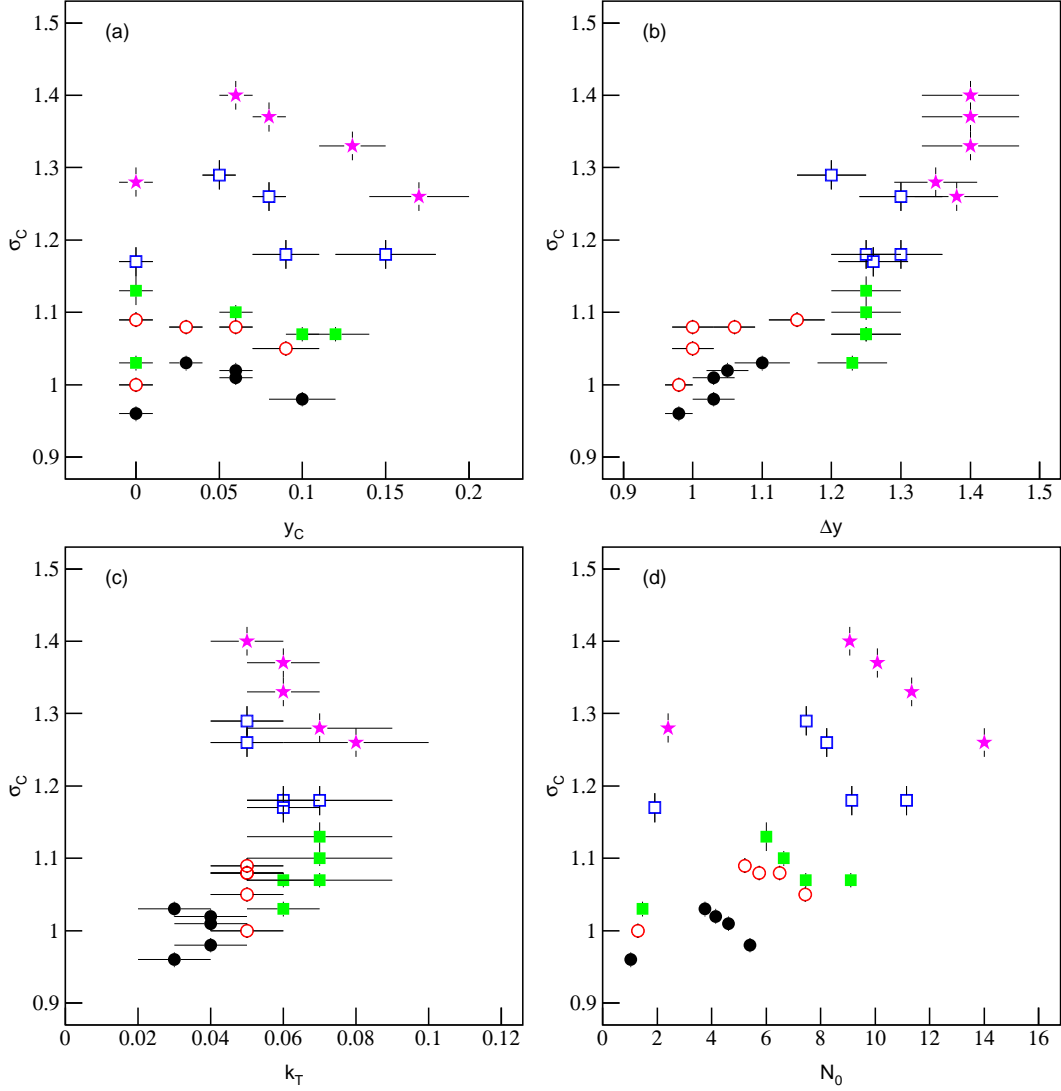


Figure 4. Dependences of σ_C on (a) y_C , (b) Δy , (c) k_T , and (d) N_0 . The symbols represent the values listed in Table 1, where the closed circles, open circles, closed squares, open squares, and stars correspond to the collision energy being 6.3, 7.7, 8.8, 12.3 (11.9), and 17.3 (16.8) GeV, respectively.

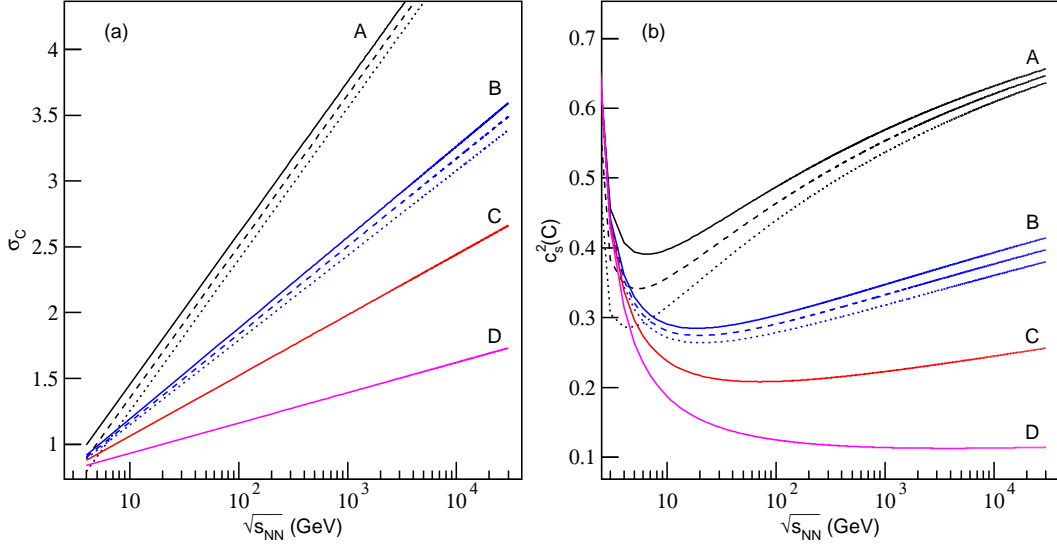


Figure 5. (a) A few examples of linear relations between σ_C and $\ln \sqrt{s_{NN}}$. (b) Different linear relations between σ_C and $\ln \sqrt{s_{NN}}$ corresponding to different dependences of $c_s^2(C)$ on $\sqrt{s_{NN}}$.

19.6 GeV, we explain it as the result of changing the mean free path of produced particles, if the statistical fluctuation is excluded. At the SPS energies, the interacting system has a small density due to low collision energy and the produced particles have a large mean free path which results from a gas-like state and results in a small c_s^2 . The situation at the RHIC or LHC energies is opposite, where the interacting system has a large density due to high collision energy and the produced particles have a small mean free path which results from a liquid-like state and results in a large c_s^2 . Let D denote the dimensionality of space. According to Refs. [36, 37], we have the relation of $c_s^2 = 1/D$ for massless particles. The particles stay at the gas-like state have a larger probability to appear in three-dimensional space, which results in the maximum c_s^2 being $1/3$ which is the situation at the SPS energies. The particles stay at the liquid-like state have a larger probability to appear in two-dimensional space, which results in the maximum c_s^2 being $1/2$ which is the situation at the RHIC and LHC energies.

To see the relations of σ_C and other parameters at the SPS energies which show the softest point in the EoS, Figures 4(a), 4(b), 4(c), and 4(d) present the dependences of σ_C on y_C , Δy , k_T , and N_0 , respectively, where the closed circles, open circles, closed squares, open squares, and stars correspond to the collision energy being 6.3, 7.7, 8.8, 12.3 (11.9), and 17.3 (16.8) GeV, respectively, which are taken from Table 1. One can see that σ_C does not show an obvious dependence on y_C and k_T , though k_T shows somehow a saturation. σ_C increases with increases of Δy and N_0 due to the latter two increasing with increase of $\sqrt{s_{NN}}$. The relation between σ_C and $\sqrt{s_{NN}}$ is the most important one among all the relations. Other relations such as the relations between σ_C and y_C , Δy , k_T , as well as N_0 are less important. To present the relations between $c_s^2(C)$ and y_C , Δy , k_T , as well as N_0 is trivial due to $c_s^2(C)$ being calculated from σ_C .

To study the most important relation between σ_C and $\sqrt{s_{NN}}$ in detail, Figure 5(a)

displays a few examples of linear relations between σ_C and $\ln \sqrt{s_{NN}}$ which reflect approximately the main area of parameter points in Figure 3(a). The solid lines corresponded to cases A, B, C, and D can be expressed by $\sigma_C = 0.5 \ln \sqrt{s_{NN}} + 0.3$, $\sigma_C = 0.3 \ln \sqrt{s_{NN}} + 0.5$, $\sigma_C = 0.2 \ln \sqrt{s_{NN}} + 0.6$, and $\sigma_C = 0.1 \ln \sqrt{s_{NN}} + 0.7$, respectively. After conversion by Eq. (3), the four similar lines of $\sigma_C - \ln \sqrt{s_{NN}}$ show very different relations of $c_s^2(C) - \ln \sqrt{s_{NN}}$ given correspondingly in Figure 5(b). Cases A and B show obvious minimums, while cases C and D do not show. Decreasing the intercept in case A from 0.3 to 0.2 and 0.1 respectively, the corresponding results presented respectively by the dashed and dotted lines in Figure 5(a) have a small change, while the results presented respectively by the dashed and dotted curves in Figure 5(b) have a large change. Decreasing the slope in case B from 0.3 to 0.29 and 0.28 respectively, the corresponding results presented respectively by the dashed and dotted lines (curves) in Figure 5(a) [5(b)] have a small change. The results presented in Figure 5 show that the minimum in Eq. (3) appearing in some special conditions.

4 Conclusions

We summarize here our main observations and conclusions.

(a) The rapidity distributions of negatively charged pions produced in p - p collisions and in ${}^7\text{Be}$ - ${}^9\text{Be}$ collisions with different centrality classes at the SPS energies are analyzed by using the revised (three-source) Landau hydrodynamic model. The model results are in agreement with the experimental data measured by the NA61/SHINE Collaboration over an energy range from 6.3 to 17.3 GeV.

(b) The values of squared speed-of-sound parameter are extracted from the widths of rapidity distributions. For the target (projectile) source, $c_s^2(T)$ [$c_s^2(P)$] decreases obviously with increase of $\sqrt{s_{NN}}$ in the considered energy range, and σ_T (σ_P) does not dependence on $\sqrt{s_{NN}}$. For the central source, $c_s^2(C)$ shows a minimum (the softest point in the EoS) at 8.8 GeV when $\sqrt{s_{NN}}$ increases from 6.3 to 17.3 GeV, and σ_C increases obviously with increase of $\sqrt{s_{NN}}$.

(c) Combining with our previous works, one can see that $c_s^2(C)$ is between 1/3 and 1/2 in most cases at higher energies (≥ 19.6 GeV). From 17.3 to 19.6 GeV, $c_s^2(C)$ has a jump from ≤ 0.3 to 1/3–1/2. In the energy range from the minimum SPS energy to the maximum LHC energy, σ_C increases monotonously with increase of $\sqrt{s_{NN}}$, though some fluctuations appear in the excitation function.

Conflict of Interests

The authors declare that there is no conflict of interests regarding the publication of this paper.

Acknowledgments

The authors would like to thank Dr. Andrzej Wilczek at University of Silesia in Katowice, Poland and Dr. Emil Aleksander Kaptur at CERN, Switzerland for supplying us the numerical data of Be-Be collisions in Figure 1 which might be a little bit different from that published in ICPAQGP-2015 [7]. This work was supported by the National

References

- [1] STAR Collaboration (J. Adams *et al.*), Phys. Rev. Lett. **95**, 062301 (2005).
- [2] PHENIX Collaboration (S.S. Adler *et al.*), Phys. Rev. C **76**, 034903 (2007).
- [3] PHOBOS Collaboration (B.B. Back, *et al.*), Phys. Rev. Lett. **87**, 102303 (2001).
- [4] ALICE Collaboration (J. Adam *et al.*), Phys. Lett. B **753**, 319 (2016).
- [5] CMS Collaboration (V. Khachatryan *et al.*), Phys. Lett. B **751**, 143 (2015).
- [6] NA61/SHINE Collaboration (N. Abgrall *et al.*), Eur. Phys. J. C **74**, 2794 (2014).
- [7] For the NA61/SHINE Collaboration (A. Wilczek), arXiv:1510.08239, Proceedings of the 7th International Conference on Physics and Astrophysics of Quark Gluon Plasma (ICPAQGP-2015), Kolkata, India, February 2–6, 2015, and private communications with A. Wilczek and E.A. Kaptur.
- [8] L.D. Landau, *Collected Papers of L. D. Landau*, D. Ter-Haarp (Ed.), p. 569, Pergamon, Oxford, UK, 1965.
- [9] S.Z. Belenkij, L.D. Landau, *Collected Papers of L.D. Landau*, D. Ter-Haarp (Ed.), p. 665, Pergamon, Oxford, UK, 1965.
- [10] I.M. Khalatnikov, J. Exp. Theor. Phys. **27**, 529 (1954).
- [11] Z.J. Jiang, H.P. Deng, Y. Zhang, H.L. Zhang, Nucl. Phys. Rev. (China) **32**, 398 (2015).
- [12] P.A. Steinberg, Nucl. Phys. A **752**, 423 (2005).
- [13] C.-Y. Wong, Phys. Rev. C **78**, 054902 (2008).
- [14] E.V. Shuryak, Yadernaya Fizika, **16**, 395 (1972).
- [15] P. Carruthers, M. Duong-Van, Phys. Rev. D **8**, 859 (1973).
- [16] P. Carruthers, Annals of the New York Academy of Sciences **229**, 91 (1974).
- [17] O.V. Zhirov, E.V. Shuryak, Yadernaya Fizika **21**, 861 (1975).
- [18] M. Gazdzickia, M. Gorensteinc, P. Seybothe, Acta Phys. Pol. B **42**, 307 (2011).
- [19] NA49 Collaboration (S.V. Afanasiev *et al.*), Phys. Rev. C **66**, 054902 (2002).
- [20] For the NA61/SHINE Collaboration (D.T. Larsen), arXiv:1510.00674.

- [21] G. Wolschin, EPL **95**, 61001 (2011).
- [22] G. Wolschin, Eur. Phys. J. A **5**, 85 (1999).
- [23] G. Wolschin, Prog. Part. Nucl. Phys. **59**, 374 (2007).
- [24] G. Wolschin, J. Phys. G **40**, 045104 (2013).
- [25] L.-N. Gao, F.-H. Liu, Adv. High Energy Phys. **2015**, 184713 (2015).
- [26] L.-N. Gao, F.-H. Liu, Adv. High Energy Phys. **2015**, 641906 (2015).
- [27] PHOBOS Collaboration (B. Alver *et al.*), Phys. Rev. C **83**, 024913 (2011).
- [28] ALICE Collaboration (E. Abbas *et al.*), Phys. Lett. B **726**, 610 (2013).
- [29] M. Bleicher, arXiv:hep-ph/0509314.
- [30] J. Steinheimer, M. Bleicher, Eur. Phys. J. A **48**, 100 (2012).
- [31] For the STAR Collaboration (L. Kumar), J. Phys. G **38**, 124145 (2011).
- [32] A. Rustamov, Cent. Eur. J. Phys. **10**, 1267 (2012).
- [33] Y.B. Ivanov and D. Blaschke, Phys. Rev. C **92**, 024916 (2015).
- [34] Y.B. Ivanov, J. Phys.: Conf. Ser. **668**, 012061 (2016).
- [35] R.A. Lacey, Phys. Rev. Lett. **114**, 142301 (2015).
- [36] K.-Y. Kim and I. Zahed, JHEP **0812**, 075 (2008).
- [37] E.I. Buchbinder, A. Buchel, and S. E. Vázquez, JHEP **0812**, 090 (2008).

Table 1. Values of free parameters, normalization constants, and χ^2/dof corresponding to the curves in Figure 1. The last two columns are the values of $c_s^2(C)$ and $c_s^2(T)$ [= $c_s^2(P)$] in the units of c^2 , where c is the speed of light in vacuum.

Figure	Type	σ_C	σ_T ($= \sigma_P$)	y_C	Δy	k_T ($= k_P$)	N_0	χ^2/dof	$c_s^2(C)$	$c_s^2(T)$ [= $c_s^2(P)$]
Figure 1(a)	p - p	0.96 ± 0.01	0.73 ± 0.01	0.00 ± 0.01	0.98 ± 0.02	0.03 ± 0.01	1.04 ± 0.01	0.284	0.266 ± 0.005	0.161 ± 0.004
	0–5%	0.98 ± 0.01	0.73 ± 0.01	0.10 ± 0.02	1.03 ± 0.03	0.04 ± 0.01	5.40 ± 0.02	6.900	0.276 ± 0.005	0.161 ± 0.004
	5–10%	1.01 ± 0.01	0.73 ± 0.01	0.06 ± 0.01	1.03 ± 0.03	0.04 ± 0.01	4.62 ± 0.01	4.419	0.290 ± 0.005	0.161 ± 0.004
	10–15%	1.02 ± 0.01	0.73 ± 0.01	0.06 ± 0.01	1.05 ± 0.03	0.04 ± 0.01	4.14 ± 0.01	3.329	0.295 ± 0.005	0.161 ± 0.004
	15–20%	1.03 ± 0.01	0.73 ± 0.01	0.03 ± 0.01	1.10 ± 0.04	0.03 ± 0.01	3.76 ± 0.01	2.494	0.300 ± 0.005	0.161 ± 0.004
Figure 1(b)	p - p	1.00 ± 0.01	0.73 ± 0.01	0.00 ± 0.01	0.98 ± 0.02	0.05 ± 0.01	1.30 ± 0.01	0.381	0.248 ± 0.004	0.138 ± 0.003
	0–5%	1.05 ± 0.01	0.73 ± 0.01	0.09 ± 0.02	1.00 ± 0.03	0.05 ± 0.01	7.44 ± 0.02	3.090	0.270 ± 0.004	0.138 ± 0.003
	5–10%	1.08 ± 0.01	0.73 ± 0.01	0.06 ± 0.01	1.00 ± 0.03	0.05 ± 0.01	6.49 ± 0.02	4.270	0.284 ± 0.005	0.138 ± 0.003
	10–15%	1.08 ± 0.01	0.73 ± 0.01	0.03 ± 0.01	1.06 ± 0.03	0.05 ± 0.01	5.75 ± 0.02	2.951	0.284 ± 0.005	0.138 ± 0.003
	15–20%	1.09 ± 0.01	0.73 ± 0.01	0.00 ± 0.01	1.15 ± 0.04	0.05 ± 0.01	5.22 ± 0.02	3.245	0.288 ± 0.005	0.138 ± 0.003
Figure 1(c)	p - p	1.03 ± 0.01	0.73 ± 0.01	0.00 ± 0.01	1.23 ± 0.05	0.06 ± 0.01	1.47 ± 0.01	1.331	0.243 ± 0.004	0.128 ± 0.004
	0–5%	1.07 ± 0.01	0.73 ± 0.01	0.12 ± 0.02	1.25 ± 0.05	0.06 ± 0.01	9.11 ± 0.02	4.870	0.260 ± 0.005	0.128 ± 0.004
	5–10%	1.07 ± 0.01	0.73 ± 0.01	0.10 ± 0.01	1.25 ± 0.05	0.07 ± 0.02	7.45 ± 0.02	2.841	0.260 ± 0.005	0.128 ± 0.004
	10–15%	1.10 ± 0.01	0.73 ± 0.01	0.06 ± 0.01	1.25 ± 0.05	0.07 ± 0.02	6.64 ± 0.02	3.001	0.272 ± 0.006	0.128 ± 0.004
	15–20%	1.13 ± 0.02	0.73 ± 0.01	0.00 ± 0.01	1.25 ± 0.05	0.07 ± 0.02	6.01 ± 0.02	5.048	0.285 ± 0.008	0.128 ± 0.004
Figure 1(d)	p - p	1.17 ± 0.02	0.73 ± 0.01	0.00 ± 0.01	1.26 ± 0.05	0.06 ± 0.01	1.91 ± 0.01	0.528	0.255 ± 0.008	0.105 ± 0.003
	0–5%	1.18 ± 0.02	0.73 ± 0.01	0.15 ± 0.03	1.25 ± 0.05	0.06 ± 0.01	11.15 ± 0.03	4.444	0.263 ± 0.008	0.107 ± 0.003
	5–10%	1.18 ± 0.02	0.73 ± 0.01	0.09 ± 0.02	1.30 ± 0.06	0.07 ± 0.02	9.15 ± 0.02	11.861	0.263 ± 0.008	0.107 ± 0.003
	10–15%	1.26 ± 0.02	0.73 ± 0.01	0.08 ± 0.01	1.30 ± 0.06	0.05 ± 0.01	8.23 ± 0.02	8.584	0.294 ± 0.008	0.107 ± 0.003
	15–20%	1.29 ± 0.02	0.73 ± 0.01	0.05 ± 0.01	1.20 ± 0.05	0.05 ± 0.01	7.48 ± 0.02	7.826	0.306 ± 0.008	0.107 ± 0.003
Figure 1(e)	p - p	1.28 ± 0.02	0.73 ± 0.01	0.00 ± 0.01	1.35 ± 0.06	0.07 ± 0.02	2.40 ± 0.01	0.912	0.258 ± 0.007	0.089 ± 0.002
	0–5%	1.26 ± 0.02	0.73 ± 0.01	0.17 ± 0.03	1.38 ± 0.06	0.08 ± 0.02	14.00 ± 0.03	8.000	0.254 ± 0.007	0.090 ± 0.002
	5–10%	1.33 ± 0.02	0.73 ± 0.01	0.13 ± 0.02	1.40 ± 0.07	0.06 ± 0.01	11.33 ± 0.03	5.009	0.279 ± 0.007	0.090 ± 0.002
	10–15%	1.37 ± 0.02	0.73 ± 0.01	0.08 ± 0.01	1.40 ± 0.07	0.06 ± 0.01	10.09 ± 0.03	2.198	0.293 ± 0.007	0.090 ± 0.002
	15–20%	1.40 ± 0.02	0.73 ± 0.01	0.06 ± 0.01	1.40 ± 0.07	0.05 ± 0.01	9.06 ± 0.02	1.567	0.304 ± 0.007	0.090 ± 0.002